

# Evaluation of bipartite entanglement between two optical multi-mode systems using mode translation symmetry

**Jun-Yi Wu and Holger F. Hofmann**

Graduate School of Advanced Sciences of Matter, Hiroshima University, Kagamiyama  
1-3-1, Higashi Hiroshima 739-8530, Japan

E-mail: junyiwu@physics.hiroshima-u.ac.jp

**Abstract.** Optical multi-mode systems provide large scale Hilbert spaces that can be accessed and controlled using single photon sources, linear optics and photon detection. Here, we consider the bipartite entanglement generated by coherently distributing  $N$  photons in  $N$  modes to two separate locations, where linear optics and photon detection is used to verify the non-classical correlations between the two  $N$ -mode systems. We show that the entangled state is symmetric under mode shift operations performed in the two systems and use this symmetry to derive correlations between photon number distributions detected after a discrete Fourier transform (DFT) of the modes. The observable correlations can be explained by a simple and intuitive rule that relates the sum of the output mode indices to the eigenvalue of the input state under the mode shift operation. Since the photon number operators after the DFT do not commute with the initial photon number operators, entanglement is necessary to achieve strong correlations in both the initial mode photon numbers and the photon numbers observed after the DFT. We can therefore derive entanglement witnesses based on the observable correlations in both photon number distributions, providing a quantitative criterion for the evaluation of large scale entanglement in optical multi-mode systems. Our method thus demonstrates how non-classical signatures in large scale optical quantum circuits can be accessed experimentally by choosing an appropriate combination of modes in which to detect the photon number distributions that characterize the quantum coherences of the state.

## 1. Introduction

The development of large scale quantum information processing in quantum optics systems [1–9] can be achieved by combining the non-classical optical fields generated by single photon sources [10–20] with increasingly complex networks of multi-mode interferometers [21–28]. It is now possible to realize large scale optical circuits by integrating optical fibers on chips or by writing the optical waveguides directly into a material by 3D printing. As a result, there has been an increasing interest in the possibilities of multi-mode interferences such as Boson sampling [29–32], multi-mode quantum metrology [26, 28, 33], as well as new methods of entanglement generation between spatially separate multi-mode systems [34]. Different from the well-studied case of two-path interferometers, the effects of a linear transformation of the modes on the photon statistics observed in the output of a multi-mode interferometer is much more difficult to characterize [35–38]. In general, the output photon statistics of a well-defined photon number input can be determined by calculating the permanent of the corresponding transformation matrix, but this is itself a NP-hard problem [35, 39, 40]. In the case of entanglement between two photonic multi-mode systems, it is therefore difficult to identify characteristic non-classical features that scale up naturally and remain easily accessible as the number of photons and modes increases. As a result, it is desirable to develop more specific theories that make use of convenient properties of the interferometers, such as symmetries between the modes.

In this paper, we address the problem of identifying the characteristic signatures of the bipartite entanglement between two multi-mode systems that is naturally generated by passing the light emitted by single photon sources through beam splitters [34]. When a large number of modes is split in this fashion and each of the output modes is distributed to two separate locations, the quantum state of the two multi-mode systems is highly entangled. However, the evaluation of the entanglement requires the performance of separate measurements of non-commuting photon distributions realized by different linear transformations of the modes. In general, the problem is that it takes complicated mathematical procedures to relate the linear transformation of modes to the resulting transformations of the Fock states representing multi-photon distributions. It is therefore necessary to develop a simple and experimentally feasible strategy to identify the specific statistical signatures that would not be possible without the entanglement. For that purpose, we propose the application of discrete Fourier transforms (DFT) to relate two sets of modes to each other by multi-mode interferometry. Although the DFT produces complicated photon number patterns by interfering all of the modes with each other, the symmetry of the operation under mode shifts allows us to classify and characterize the patterns in a manner that enables us to efficiently identify the effects of entanglement experimentally. Specifically, the mode shift symmetry of the DFT converts a cyclic shift of the input mode indices into a well-defined phase shift of the output modes. This useful property of the modes can be applied directly to the transformation of photon number states, resulting in a simple relation between the two representations

of the quantum state which we call the mode shift rule of DFTs. This mode shift rule identifies the quantum coherences between different input photon numbers of the DFT with sets of photon number distributions in the output, allowing us to identify the effects of quantum coherences in the entangled input state on the correlations between photon number patterns observed after the DFT has been applied to both multi-mode systems. Based on this fundamental insight into the relation between photon number distributions before and after the DFT, we can then derive experimental criteria for the verification of entanglement between two multi-mode systems of arbitrary size and photon numbers.

The remainder of the paper is organized as follows. In section 2, we discuss generation of the entangled system between two local  $M$ -mode systems  $A$  and  $B$  obtained from beam splitting  $M$  single photon input modes. In section 3, the generated state is projected onto the subspaces by post-selecting the photon distributions measured by photon detectors with fixed local photon number partitions  $(N_A, N_B)$ . In section 4, we identify the DFT of the optical modes as the most promising linear transformation for the complementary measurements in the local multi-mode systems. In section 5, we derive the mode shift rule of DFTs for multi-mode systems. In section 6, we employ the mode shift rule to formulate an experimentally observable criterion for entanglement verifications by identifying the bounds of correlation fidelities that apply to all separable states of the two multi-mode systems. In section 7, we optimize the bound by including the classification of photon number distributions observed in the original input modes into pattern classes. Finally, we apply the analysis to the specific example of 4-mode single photon inputs split into two local 4-mode systems with 2 photons each (section 8) and conclude the paper (section 9).

## 2. Entanglement from multi-mode beam splitting

Multi-mode systems can be characterized experimentally by photon number detection. Ideally, it is possible to assign a specific photon number  $n_m$  to each mode  $m$ , so that the observed photon number distribution can be given by an array

$$\mathbf{n} = (n_0, \dots, n_{M-1}), \quad (1)$$

where the modes are indexed by  $\{0, \dots, M-1\}$ . Since the photon numbers are eigenvalues of the  $M$  harmonic oscillator modes, each photon number distribution corresponds to a well defined energy eigenstate  $|\mathbf{n}\rangle$  in the Fock space of the  $M$ -mode system.

Entangled states of two  $M$ -mode systems can be described by a superposition of photon number states  $|\mathbf{n}_A\rangle |\mathbf{n}_B\rangle$ , where the photon number patterns  $\mathbf{n}_A$  are correlated with the photon number patterns  $\mathbf{n}_B$ . The simplest example is a single photon passing through a beam splitter, which results in a coherent superposition of the photon number state  $|1_A\rangle |0_B\rangle$  where the photon is found in  $A$ , and the photon number state  $|0_A\rangle |1_B\rangle$  where the photon is found in  $B$ . Technically, this superposition is a maximally entangled Bell state of the local modes at  $A$  and at  $B$  given by  $(|1_A\rangle |0_B\rangle + |0_A\rangle |1_B\rangle)/\sqrt{2}$  [41–45].

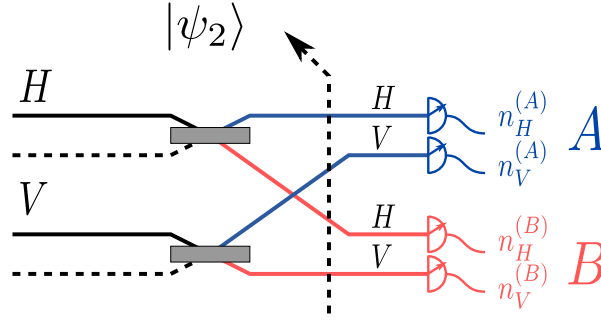


**Figure 1.** The schematic setup of entanglement generation between two 2-mode systems in [46]. Two single photons in the  $\{H, V\}$  polarization modes are generated from a down conversion source, and distributed by beam splitters into two local system with the modes  $\{H_A, V_A\}$  and  $\{H_B, V_B\}$ , respectively. The state  $|\psi_2\rangle$  after the beam splitting is given in Eq. (2). By post-selecting one-photon detection events in each local system, one projects the  $|\psi_2\rangle$  onto the entangled state  $|\phi_{1_A, 1_B}\rangle$  in Eq. (3).

However, photon detection can only access the  $\{|0\rangle, |1\rangle\}$  basis, making it impossible to observe the entanglement without additional ancillary photon sources.

Conveniently, the situation changes when this system is scaled up by combining multiple single photon inputs, distributing them to the multi-mode systems  $A$  and  $B$ . A well known example is the generation of entangled pairs used in one of the earliest experiments of entanglement generation by Ou and Mandel [46], where two orthogonal modes are split by two beam splitters and the 4 output modes are separated into two local systems with two modes each (see Fig. 1). Two single photons are generated in the modes  $\{H, V\}$  and then distributed into the local systems  $A$  and  $B$  by the beam splitters, resulting in the state

$$|\psi_2\rangle = \frac{1}{2}(|00\rangle_A |11\rangle_B + |11\rangle_A |00\rangle_B + |01\rangle_A |10\rangle_B + |10\rangle_A |01\rangle_B). \quad (2)$$

By post-selection of the outcomes with only one photon in each local system, one can obtain the two photon Bell state

$$|\phi_{1_A, 1_B}\rangle = \frac{1}{\sqrt{2}}(|01\rangle_A |10\rangle_B + |10\rangle_A |01\rangle_B). \quad (3)$$

As is well known, it is easy to access the entanglement of this state using linear optics and photon detection, since the two-mode transformations of linear optics map directly onto the Bloch sphere of the two-level single photon systems.

It is a straightforward matter to scale up the procedure of generating bipartite entanglement by beam splitting to general  $M \otimes M$ -mode systems [34]. As shown in Fig. 2,  $M$  photons in  $M$  input modes can be split by  $M$  beam splitters and distributed into two separate locations  $A$  and  $B$ . Each local system then has  $M$  modes described by mode indices  $m = 0, \dots, M - 1$  that correspond to the mode index of the input mode from which they originated. One can use linear optics transformations on each of the local  $M$ -mode systems to implement local unitaries  $U_A$  and  $U_B$ . These local unitaries

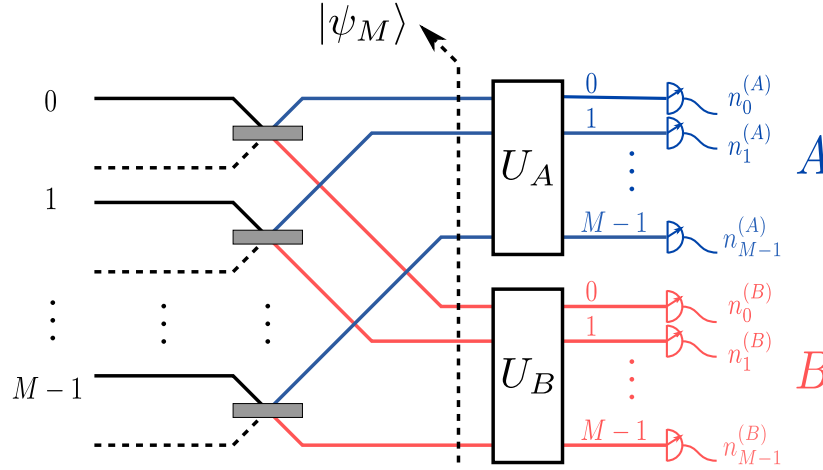


**Figure 2.** Generation of bipartite entanglement from  $M$  single photon inputs and its evaluation. The input modes and the modes in each output port are indexed by  $0, \dots, M-1$ . The  $M$  single photon inputs are split by  $M$  beam splitters.  $|\psi_M\rangle$  is the state before the local unitary transformations  $U_A$ ,  $U_B$  and photon detections.

change the measurement basis of photon detection by transforming the modes in which the photons are detected. Since the photon number distributions in the output of different linear optics transformations do not commute with each other, it is in principle possible to verify entanglement by observing correlations in different non-commuting output distributions which can exceed the limits valid for separable states.

Since the photon in input mode  $m$  will either appear in the corresponding mode  $m$  of port  $A$  or in the corresponding mode  $m$  of port  $B$ , the state  $|\psi_M\rangle$  obtained after the photons have been distributed to  $A$  and  $B$  is given by a coherent superposition of all possible photon number states  $|\mathbf{n}_A\rangle |\mathbf{n}_B\rangle$  satisfying the complementary correlation  $\mathbf{n}_A + \mathbf{n}_B = (1, \dots, 1)$ ,

$$|\psi_M\rangle = \left( \frac{1}{\sqrt{2}} (|1\rangle_A |0\rangle_B + |0\rangle_A |1\rangle_B) \right)^{\otimes M} = \frac{1}{2^{M/2}} \sum_{n_m \leq 1} |\mathbf{n}\rangle_A |\bar{\mathbf{n}}\rangle_B, \quad (4)$$

where  $\mathbf{n}$  are the  $M$ -dimensional vectors describing the photon number distribution in the  $M$  modes. Each vector represents a specific distribution pattern, and in general,  $n$  could take any value from 0 to  $M$ . However, the input patterns are restricted to patterns with  $n = 0$  or  $n = 1$ , so that it is possible to define the complementary pattern  $\bar{\mathbf{n}}$  as  $(1, \dots, 1) - \mathbf{n}$ . Consequently, the sum in Eq.(4) runs over all  $M$ -mode patterns with maximally one photon in each mode.

The state  $|\psi_M\rangle$  exists in a Hilbert space that includes many different photon number distributions between system  $A$  and system  $B$ . However, linear optics and photon detection will always identify the precise value of the local photon number. It is therefore not possible to access the coherences between subspaces with different local photon numbers without using additional resources such as weak coherent input fields. For practical reasons, it is therefore useful to distinguish the total photon numbers in

the local systems before analyzing the entanglement that can be observed by detecting the precise distribution of photons within each local  $M$ -mode system.

### 3. Distribution of photons between $A$ and $B$

Linear optics transformations always conserve the total photon number. This means that, no matter what linear optics transformation we chose, the total output photon number at the detectors remains the same. Conversely, it also means that linear optics and photon number detection is never sensitive to quantum coherences between states of different total photon number. We can therefore classify the measurements performed by linear optics and photon detection according to the total photon number  $N$  detected in the output. If  $\hat{\Pi}_M^N$  is the projector on the  $M$ -mode Fock states with a total photon number of  $N$ , we can express each measurement as a sequence of projection on total photon number, unitary transformation, and final detection of the specific photon number distribution,

$$|\langle \mathbf{n} | \hat{U}_{\text{lin.}} | \psi \rangle|^2 = |\langle \mathbf{n} | \hat{U}_{\text{lin.}} \hat{\Pi}_M^N | \psi \rangle|^2. \quad (5)$$

Since the operator  $\hat{\Pi}_M^N$  can be applied to the input state  $|\psi\rangle$  before the linear optics mode transformation, it is sufficient to consider the quantum statistics of the reduced state  $\hat{\Pi}_M^N |\psi\rangle$  by itself, separate from the components with different total photon numbers. In the case of the entangled state  $|\psi_M\rangle$ , we can apply the same reasoning to both local systems and make use of the fact that the total photon number is  $M$ . The probabilities for a specific set of detection patterns are then given by the probabilities

$$P(\mathbf{n}_A, \mathbf{n}_B) = |\langle \mathbf{n}_A \mathbf{n}_B | (\hat{U}_{\text{lin.}}^{(A)} \otimes \hat{U}_{\text{lin.}}^{(B)}) (\hat{\Pi}_M^N \otimes \hat{\Pi}_M^{M-N}) | \psi_M \rangle|^2, \quad (6)$$

where  $N$  is the total photon number detected in  $A$  and  $M - N$  is the total photon number detected in  $B$ . Since any photon detection measurement clearly distinguishes between the different partitions of photon numbers between  $A$  and  $B$ , it is useful to characterize the quantum state components associated with each partition separately.

The probability of obtaining a photon number partition of  $(N, M - N)$  is given directly by the expectation value of the projectors and is easily obtained from the binomial statistics introduced by the beam splitters that distribute the photons to  $A$  or  $B$ ,

$$P(N, M - N) = \langle \psi_M | \hat{\Pi}_M^N \otimes \hat{\Pi}_M^{M-N} | \psi_M \rangle = \frac{1}{2^M} \binom{M}{N}. \quad (7)$$

If we use the total photon number as a fixed condition in the evaluation of the entanglement, we can convert the measurement probabilities  $P(\mathbf{n}_A, \mathbf{n}_B)$  into conditional probabilities by dividing them by  $P(N, M - N)$ . The measurement probabilities for specific patterns  $(\mathbf{n}_A, \mathbf{n}_B)$  with  $|\mathbf{n}_A| = N$  and  $|\mathbf{n}_B| = (M - N)$  are then obtained directly from the normalized quantum state in the  $(N, M - N)$  subspace, which is given by

$$|\phi_{N, M-N}\rangle = \frac{1}{\sqrt{P(N, M - N)}} \hat{\Pi}_M^N \otimes \hat{\Pi}_M^{M-N} |\psi_M\rangle. \quad (8)$$

Effectively, we can always post-select the state  $|\phi_{N,M-N}\rangle$  in any measurement that identifies the total photon number in  $A$  and in  $B$ . We can therefore simplify our analysis by looking at the entanglement of one post-selected state at a time. It should be noted that the state  $|\phi_{N,M-N}\rangle$  is still an entangled state of two multi-photon  $M$ -mode systems. In fact, the post-selection does not change the structure of the entangled state much, as can be seen when it is expressed in the input mode photon number basis,

$$|\phi_{N,M-N}\rangle = \frac{1}{\sqrt{\binom{M}{N}}} \sum_{n_m \leq 1, |\mathbf{n}|=N} |\mathbf{n}\rangle |\bar{\mathbf{n}}\rangle. \quad (9)$$

The entanglement is still expressed by perfect correlations between the input patterns in  $A$  and their complementary patterns in  $B$ , and the only change with regard to the original state is that the sum runs only over patterns that have exactly  $N$  photons in system  $A$ .

The post-selected states are maximally entangled in a Hilbert space of dimension  $\binom{M}{N}$ , as compared to the original entanglement with a Schmidt rank of  $2^M$ . Specifically, the original  $2^M$ -dimensional entanglement is divided up into  $M+1$  different components  $|\phi_{N,M-N}\rangle$  of which all except the one-dimensional cases of  $N=0$  and  $N=M$  are entangled states. The two separable states  $|\phi_{0,M}\rangle$  and  $|\phi_{M,0}\rangle$  both have a probability of  $1/2^M$ , which falls off exponentially as the input photon number  $M$  increases. In general, the Schmidt rank of all entangled states  $|\phi_{N,M-N}\rangle$  is proportional to the probability of detecting the state  $|\phi_{N,M-N}\rangle$  in the input  $|\psi_M\rangle$ . This means that the probability of detecting a state actually increases with the amount of entanglement in that state. The states with the highest probabilities  $P(N, M-N)$  are the states with nearly equal photon numbers in  $A$  and  $B$ . For high input photon numbers  $M$ , this probability can be approximated by a Gaussian distribution,

$$P(N, M-N) \approx \sqrt{\frac{2}{\pi M}} \exp\left(-\frac{2}{M}\left(N - \frac{M}{2}\right)^2\right). \quad (10)$$

The Schmidt rank of each photon number partition is given by  $2^M P(N, M-N)$ , indicating that the vast majority of post-selected states have high amounts of entanglement. Since the Schmidt rank of the complete input state is  $2^M$ , the maximal probability of  $P(M/2, M/2)$  is a good estimate of the expected reduction of Schmidt rank caused by the use of linear optics and photon detection. As can be seen from Eq. (10), this reduction ratio scales with the square root of  $M$ , which is nearly negligible when compared to the exponential scaling of the overall Schmidt rank. We can therefore conclude that the limitation to linear optics and photon detection reduces the amount of available entanglement only slightly while greatly reducing the technological effort involved in the characterization and application of the entangled state. In the following, we will take a closer look at the possible measurements that can be performed using these basic optical technologies.

#### 4. Transformation of photon number states by linear optics

In principle, linear optics is sufficient to transform a photon number state in the input into coherent superpositions of photon number states in the output. It is therefore possible to characterize the non-classical correlations of each entangled state  $|\phi_{N,M-N}\rangle$  using only linear optics and photon detection. If we wish to describe the output photon number distribution in output modes  $k$  in terms of the input photon number distributions in input modes  $m$ , it is convenient to describe the linear optics transformation using the unitary  $M \times M$  matrix that describes the transformations of the  $M$  creation operators associated with the coherent field amplitudes of the modes,

$$\hat{U}_{\text{lin.}}^\dagger \hat{a}_k^\dagger \hat{U}_{\text{lin.}} = \sum_{m=0}^{M-1} T_{km}^* \hat{a}_m^\dagger. \quad (11)$$

In terms of photon number distributions, the coefficients  $T_{km}$  represent the possibility of a photon transfer from mode  $m$  to mode  $k$ . However, quantum interference effects modify this probability, making it a non-trivial task to determine the complete multi-photon statistics of linear optics transformations. Specifically, quantum interference results in photon bunching effects, which results in a preference for output patterns with multiple photons in the same mode. We can therefore conclude that a linear optics transformation applied to an input photon number state with at most one photon in each mode is likely to result in output photon number distributions with more than one photon in each mode. For the entangled states  $|\phi_{N,M-N}\rangle$ , this means that only the photon number distribution in the original input modes is limited to the  $\binom{M}{N}$  distribution patterns with  $n_m \leq 1$ . All other multi-photon measurements cover the complete Hilbert spaces of  $N$  photons in  $M$  modes for  $A$  and  $M - N$  photons in  $M$  modes for  $B$ . It is therefore a non-trivial task to identify correlations between the different kinds of photon number distributions observed in system  $A$  and in system  $B$ .

Next, we consider which linear optics transformation is most sensitive to the non-classical correlations of  $|\phi_{N,M-N}\rangle$ . Since the entanglement we have generated is perfectly symmetric in the  $M$  input modes, the optimal results should be obtained by using linear optics transformations that interfere equal fractions of each input mode with each other, resulting in a unitary matrix with  $|T_{km}|^2 = 1/M$ . In addition, we need a transformation that is easy to apply to any number of modes. By combining these two requirements, we arrive at the discrete Fourier transform (DFT)  $\hat{U}_{\text{F}}$ , given by

$$\hat{U}_{\text{F}}^\dagger \hat{a}_k^\dagger \hat{U}_{\text{F}} = \sum_{m=0}^{M-1} \frac{1}{\sqrt{M}} e^{-i\frac{2\pi}{M}km} \hat{a}_m^\dagger. \quad (12)$$

For single photon states, the condition that all modes interfere equally corresponds to the requirement that the input photon number basis is mapped onto a mutually unbiased output basis. However, the results for multi-photon input states involve quantum interferences and photon bunching effects that result in a more complicated relation



between the input basis and the output basis. In the following, we will simplify the analysis of output photon number distributions of the DFT by taking a closer look at the symmetry between the input modes and its effects on the relation between input and output in the DFT.

## 5. Eigenstates of the mode shift operation

The DFT in Eq. 12 is based on a cyclic ordering of the modes given by the mode index  $m$  which is a modular value running from  $m = 0$  to  $m = M - 1$ . This ordering of the modes can be used to define a cyclic mode shift operation which transforms the creation operator of the  $m$ -th mode creation operator into the creation operator of the  $(m + 1)$ -th mode,

$$\hat{S}a_m^\dagger\hat{S}^\dagger = a_{m+1}^\dagger, \quad (13)$$

where  $m$  is modular in  $M$ , so that  $\hat{a}_{M-1}^\dagger$  is transformed into  $\hat{a}_0^\dagger$ . When applied directly to a photon number state, the mode shift operator simply moves the photon number distribution accordingly, e.g.  $\hat{S}^2|110\rangle = \hat{S}|011\rangle = |101\rangle$ . One can then identify sets of cyclic patterns  $\mathcal{E}_{\mathbf{p}}$ , such that all of the states in the set can be transformed into each other by multiple applications of the shift operation  $\hat{S}$ ,

$$\mathcal{E}_{\mathbf{p}} = \{\hat{S}^m|\mathbf{p}\rangle\}. \quad (14)$$

The whole set can then be identified by a single representative photon number distribution pattern  $\mathbf{p}$ . In the following, we will refer to the set of states  $\mathcal{E}_{\mathbf{p}}$  as the pattern class  $\mathbf{p}$ . Note that the cardinality of most pattern classes is  $M$ , since it usually takes  $M$  applications of  $\hat{S}$  to return to the original pattern. However, some pattern classes have a lower cardinality because the symmetry of the original pattern reduces the number of shifts needed to return to the original pattern, resulting in integer fractions of the original cardinality,  $M/2$ ,  $M/3$ , and so on. For example, the pattern class  $\mathcal{E}_{1010} = \{|1010\rangle, |0101\rangle\}$  has a cardinality of  $M/2 = 2$  since only two shifts are needed to return the pattern 1010 to itself. The Hilbert subspace spanned by the photon number basis  $\mathcal{E}_{\mathbf{p}}$  in  $\mathbf{p}$ -pattern class will be denoted as  $\mathbb{H}_{\mathbf{p}}$  in the rest of this paper, while the cardinality of a pattern class is denoted by  $d_{\mathbf{p}}$ .

We can now consider the effect of a mode shift operation performed in the input of a DFT on the output photon number distributions observed after the DFT. According to the relation between input creation operators and output creation operators described in Eq.(12), the effect of the output mode shift operation is given by

$$\hat{S}\left(\hat{U}_{\text{F}}^\dagger\hat{a}_k^\dagger\hat{U}_{\text{F}}\right)\hat{S}^\dagger = e^{i\frac{2\pi}{M}k}\left(\hat{U}_{\text{F}}^\dagger\hat{a}_k^\dagger\hat{U}_{\text{F}}\right). \quad (15)$$

Thus, the mode shift operation performed in the input of the DFT results in a phase shift for each output mode  $k$ . Specifically, the phase shift is given by  $2\pi k/M$ , which is proportional to the mode index  $k$ . Since the eigenstates of a phase shift in a given mode are the photon number states of that mode, the multi-photon output states of the

DFT  $U_F^\dagger |\mathbf{n}\rangle$  are eigenstates of the mode shift operator  $\hat{S}$  applied before the DFT. The eigenvalues of the output states  $U_F^\dagger |\mathbf{n}\rangle$  can be found by multiplying the phase factors associated with each creation operator  $\hat{a}_k$ , resulting in an accumulated total phase shift given by the sum of the single photon  $k$  values,

$$\hat{S} \hat{U}_F^\dagger |\mathbf{n}\rangle = e^{i\frac{2\pi}{M}K(\mathbf{n})} \hat{U}_F^\dagger |\mathbf{n}\rangle \quad (16)$$

with

$$K(\mathbf{n}) = \sum_{k=0,\dots,M-1} n_k k \pmod{M}. \quad (17)$$

Here,  $K(\mathbf{n})$  is the modular value of the total mode index of the photon number state  $|\mathbf{n}\rangle$ . A value of  $K = 0$  indicates that the pattern is centered around the  $k = 0$  mode, so that for any photon shifted to a higher  $k$  value, another photon is shifted to a lower  $k$  value. A non-zero  $K$  value can be obtained by shifting one of the photons in a  $K = 0$  pattern to the next higher mode. The  $K$  value is therefore a measure of the total unbalanced mode shifts in the distribution of photons over the output modes. For example, the patterns 0101, 2000 and 0020 are symmetrically distributed around the 0-th mode and have a total value of  $K = 0$ , while the patterns 0011, 1100 can be obtained by shifting one photon in the  $K = 0$  patterns to the next mode and therefore have a total value of  $K = 1$ .

Since the photon number eigenstates detected after a DFT has been performed on the initial input modes are eigenstates of the mode shift operation applied to the input, the output photon numbers of the DFT are conserved under mode shift operations. This means that the statistics of the measurement outcomes detected after the DFT are not changed by the mode shift operation on the input. For any input state  $|\psi\rangle$ ,

$$|\langle \mathbf{n} | \hat{U}_F \hat{S}^m | \psi \rangle|^2 = |\langle \mathbf{n} | \hat{U}_F | \psi \rangle|^2, \quad (18)$$

where  $m$  is a completely arbitrary integer. This relation has direct implications for the cyclic pattern classes  $\mathcal{E}_{\mathbf{p}}$ , since the elements in these classes are related to each other by input mode shifts. We can therefore conclude that each state in a pattern class produces the same output statistics after the DFT is applied to it, which means that photon detection after the DFT cannot distinguish between different input states from the same pattern class. Instead, the photon detection after DFT determines the  $K$  value associated with the eigenvalue  $\exp(i2\pi K/M)$  of the mode shift operation  $\hat{S}$ . By considering only the  $K$  value of the output photon number distribution observed in the experiment, we can identify the corresponding eigenstate within each of the Hilbert spaces spanned by the elements of a specific cyclic pattern class  $\mathcal{E}_{\mathbf{p}}$ . It should be noted that these eigenstates do not correspond to the photon number states detected after the DFT. However, they are part of the eigenspace spanned by all photon number states with the same  $K$  value, so that they can be represented by a superposition of measurement outcomes characterized by the same experimentally observable  $K$ . It is therefore possible to experimentally distinguish between the different  $K$ -values within

a given cyclic pattern class even though it is not possible to directly project onto the  $K$ -eigenstate of that particular pattern class.

We can define the eigenstates of the mode shift operation  $\hat{S}$  within the Hilbert space spanned by the cyclic pattern class  $\mathcal{E}_{\mathbf{p}}$  as

$$\hat{S} |\mathcal{E}_{\mathbf{p}}, K\rangle = e^{i\frac{2\pi}{M}K} |\mathcal{E}_{\mathbf{p}}, K\rangle. \quad (19)$$

Since the application of a mode shift operation on each element of the pattern class produces the next element in the class, the eigenstates are equal superpositions of all the elements in the class, where the phases are determined by  $K$ . the conservation of the statistics of  $|\langle \mathcal{E}_{\mathbf{p}}, k | \hat{U}_{\mathbf{F}}^\dagger \hat{S}^m | \mathbf{p} \rangle|^2$  in the mode shifting operation must holds analogously to Eq. (18) and the  $\hat{S}$ -eigenstates must be therefore the equal superposition of all the elements of the  $\mathbf{p}$ -pattern class with the phase  $\exp(-i2\pi Km/M)$ ,

$$|\mathcal{E}_{\mathbf{p}}, K\rangle := \frac{1}{\sqrt{d_{\mathbf{p}}}} \sum_{m=0}^{d_{\mathbf{p}}-1} e^{-i\frac{2\pi}{M}Km} \hat{S}^m |\mathbf{p}\rangle, \quad (20)$$

where  $d_{\mathbf{p}}$  is the cardinality the  $\mathbf{p}$ -pattern class, and the  $K$  values depends on the cardinality  $d_{\mathbf{p}}$  and are multiples of  $M/d_{\mathbf{p}}$ ,

$$K = 0, \frac{M}{d_{\mathbf{p}}}, 2\frac{M}{d_{\mathbf{p}}}, \dots, M - \frac{M}{d_{\mathbf{p}}}. \quad (21)$$

The set of  $\mathbf{p}$ -pattern  $\hat{S}$ -eigenstates is a basis of the  $\mathbf{p}$ -pattern subspace  $\mathbb{H}_{\mathbf{p}}$ , which is denoted by

$$\mathcal{K}_{\mathbf{p}} = \{|\mathcal{E}_{\mathbf{p}}, K\rangle\}_K. \quad (22)$$

For example, the  $\hat{S}$ -eigenstates of the 1010-pattern class are  $\mathcal{K}_{1010} = \{|\mathcal{E}_{1010}, 0\rangle, |\mathcal{E}_{1010}, 2\rangle\}$  with

$$|\mathcal{E}_{1010}, 0\rangle = \frac{1}{\sqrt{2}}(|1010\rangle + |0101\rangle) \quad |\mathcal{E}_{1010}, 2\rangle = \frac{1}{\sqrt{2}}(|1010\rangle - |0101\rangle). \quad (23)$$

As shown in Eq. (20), a  $\mathbf{p}$ -pattern  $\hat{S}$ -eigenstate is given by an equal superposition of the  $\mathbf{p}$ -pattern photon number states. Likewise, each photon number state in the  $\mathbf{p}$ -pattern class can be expressed by an equal superposition of  $\mathbf{p}$ -pattern  $\hat{S}$ -eigenstates. Therefore  $\mathcal{E}_{\mathbf{p}}$  and  $\mathcal{K}_{\mathbf{p}}$  are two mutually unbiased bases (MUBs) of the  $\mathbf{p}$ -pattern subspace  $\mathbb{H}_{\mathbf{p}}$ .

We can now clarify the relation between the photon number statics  $\mathbf{n}$  observed after the DFT and the  $K$ -value eigenstates  $|\mathcal{E}_{\mathbf{p}}, K\rangle$  of the cyclic pattern classes  $\mathbf{p}$ . Effectively, the total Hilbert space can be separated into the highly degenerate eigenspaces of  $\hat{S}$  associated with different  $K$ -values. Both the DFT output states  $\{U_{\mathbf{F}}^\dagger |\mathbf{n}\rangle\}$  with  $K(\mathbf{n}) = K$  and the states  $\{|\mathcal{E}_{\mathbf{p}}, K\rangle\}$  of the different cyclic pattern classes  $\mathbf{p}$  form complete basis sets of these eigenspaces. The transformations between these two basis sets is given by

$$\langle \mathbf{n} | \hat{U}_{\mathbf{F}} | \mathcal{E}_{\mathbf{p}}, K' \rangle = c_{(\mathbf{n}, \mathbf{p})} \delta_{K(\mathbf{n}), K'}, \quad (24)$$

where the basis states associated with different subspaces are always orthogonal. Note that the coefficients  $c_{(\mathbf{n}, \mathbf{p})}$  can be used to express the measurement outcome  $\{U_F^\dagger |\mathbf{n}\rangle\}$  as a superposition of pattern class states  $|\mathcal{E}_{\mathbf{p}}, K\rangle$ ,

$$\hat{U}_F^\dagger |\mathbf{n}\rangle = \sum_{\mathbf{p}} c_{(\mathbf{n}, \mathbf{p})} |\mathcal{E}_{\mathbf{p}}, K(\mathbf{n})\rangle. \quad (25)$$

The measurement outcome  $\mathbf{n}$  thus selects a single state from each pattern class  $\mathbf{p}$ , and this state is represented by an equal superposition of the input photon number states.

We summarize these results by formulating the *mode shift rule of DFTs*, which states that the  $K$ -values of photon number distributions obtained in the output of a DFT always distinguish the different eigenspaces of a mode shift operation in the input, regardless of the other details of the output photon number patterns. It is therefore possible to identify the coherence between elements of a pattern class even if we do not know which pattern class we observed. To apply the rule, one needs to calculate the  $K$ -value from the output photon number distribution of the DFT using Eq.(17). It is then possible to identify the coherence between the elements of each pattern class, since according to Eqs. (20) and (25), the  $K$ -value alone determines the coherence between the elements of the cyclic pattern classes  $\mathcal{E}_{\mathbf{p}}$ . Note that the mode shift rule can be viewed as a generalization of the suppression laws of DFTs [36, 47], which predict zero probability for output patterns of cyclic periodically symmetric input photon number states. This suppression can now be obtained from the mode shift rule for the  $\hat{S}$ -eigenstates with  $K = 0$ . For the evaluation of multi-mode entanglement by the correlations of outputs after local DFTs, the general mode shift rule is needed to evaluate the quantum coherence between photon number components.

An important corollary of the mode shift rule of DFTs is that any statistical bias in favor of a specific  $K$ -value is an indicator of quantum coherences between different input photon number distributions. The  $K$ -values obtained in the output of the DFT can therefore be used as evidence of quantum coherence between photon number states in the input. In the following, we will apply this rule to the analysis of multi-mode entanglement based on the correlations between the  $K$ -values observed after the DFT.

## 6. Entanglement criterion

The merit of applying the mode shift rule to the analysis of the photon number statistics observed after a DFT is that the large amount of information in the photon number distribution  $\mathbf{n}$  obtained in the output measurement can be reduced to a single  $K$ -value using Eq.(17). In the case of the entangled state  $|\phi_{N, M-N}\rangle$  between two multi-mode systems of different local photon numbers  $N$  and  $M - N$ , this makes it possible to efficiently analyze correlations between a wide variety of very different photon number distributions observed at  $A$  and at  $B$ .

The application of the DFT to characterize the entangled state  $|\phi_{N, M-N}\rangle$  is motivated by the fact that the beam splitting procedure is completely symmetric in

the modes  $M$ , so that a rearrangement of mode labels has no effect whatsoever on the entangled state, as long as the labels in system  $A$  correspond to the labels in system  $B$ . It is therefore obvious that a simultaneous mode shift operation performed in  $A$  and in  $B$  does not change the state at all, making  $|\phi_{N,M-N}\rangle$  an eigenstate of this operation with an eigenvalue of one,

$$\hat{S}^{(A)} \otimes \hat{S}^{(B)} |\phi_{N,M-N}\rangle = |\phi_{N,M-N}\rangle. \quad (26)$$

If the entangled state  $|\phi_{N,M-N}\rangle$  is represented by a superposition of local eigenstates of the mode shift operations, each component must independently satisfy the eigenvalue relation, which means that the product of the eigenvalues of the local mode shift operations must be one. It is easy to see that this requires that the modular sum of the  $K$ -values must be zero, so that  $K_A + K_B = 0 \pmod{M}$ . Within each pattern class, the perfect correlation between input photon number patterns therefore transforms into a perfect correlation between  $K$ -values, so that the entangled state for total photon numbers of  $N$  and  $M - N$  can be written as

$$|\phi_{N,M-N}\rangle = \frac{1}{\sqrt{\binom{M}{N}}} \sum_{\mathbf{p} \in \mathcal{P}_\phi^{(A)}} \sum_{|\mathcal{E}_{\mathbf{p},k} \in \mathcal{K}_{\mathbf{p}}} |\mathcal{E}_{\mathbf{p},K}\rangle |\mathcal{E}_{\bar{\mathbf{p}},-K}\rangle, \quad (27)$$

where  $\mathcal{P}_\phi^{(A)}$  denotes the set of pattern classes of  $N$  photons with zero or one photon in each mode and  $\bar{\mathbf{p}}$  is the complementary pattern class, obtained by exchanging zero photon with one photon and vice versa.

Within each pattern class subspace, the eigenstates of the mode shift operators and the photon number states are mutually unbiased. This means that separable states can only be correlated in either the  $K$ -values or in the photon number distributions. The observation of both  $K$ -correlations ( $K, -K$ ) in the outputs of the DFT and the complementary correlations ( $\mathbf{n}, \bar{\mathbf{n}}$ ) in the original photon number basis is an experimentally accessible signature of the entanglement between  $A$  and  $B$ . It is thus possible to verify the entanglement of the state  $|\phi_{N,M-N}\rangle$  by quantifying the experimentally observed correlations in the two measurements described by  $|\mathbf{n}\rangle$  and  $\hat{U}_F^\dagger |\mathbf{n}\rangle$ . If these correlations exceed the bound satisfied by all separable states, the experimental data confirms the successful generation of entanglement between the multi photon systems at  $A$  and at  $B$ .

The correlations in the photon detection in the input modes can be quantified by the  $\mathbf{n}$ -correlation fidelity  $F_{\mathbf{n}}$ , which is given by the probability of observing the expected ( $\mathbf{n}, \bar{\mathbf{n}}$ )-correlation between the outputs at  $A$  and at  $B$ . By summing over the probability of all correctly correlated combinations of photon number distributions, we obtain

$$F_{\mathbf{n}} = \sum_{n_m \leq 1} \langle \mathbf{n} \bar{\mathbf{n}} | \hat{\rho}_{\text{exp.}} | \mathbf{n} \bar{\mathbf{n}} \rangle, \quad (28)$$

where  $\hat{\rho}_{\text{exp.}}$  is the density operator of the experimentally generated state. Similarly, the correlations between the  $K$ -values of the photon number distributions detected after

DFTs have been performed in both systems can be quantified by the  $K$ -correlation fidelity  $F_K$ , which is given by the probability of observing the correct  $(K, -K)$ -correlation between the outputs at  $A$  and at  $B$ . By summing over the probability of all correctly correlated combinations of photon number distributions, we obtain

$$F_K = \sum_{K(\mathbf{n}_A) + K(\mathbf{n}_B) = 0} \langle \mathbf{n}_A \mathbf{n}_B | \hat{U}_F \otimes \hat{U}_F \hat{\rho}_{\text{exp.}} \hat{U}_F^\dagger \otimes \hat{U}_F^\dagger | \mathbf{n}_A \mathbf{n}_B \rangle, \quad (29)$$

where  $K_A, K_B$  are the  $K$ -values associated with the photon number distributions  $\mathbf{n}_A, \mathbf{n}_B$  respectively.

For the ideal entangled state, these fidelities are both equal to 1, achieving the maximal value of 2 for the sum of both fidelities. To obtain a quantitative criterion for experimental entanglement detection, we have to identify the upper bound of the fidelity sum for separable states. To do so, it is helpful to express the fidelities as expectation values of operators,

$$F_{\mathbf{n}} + F_K = \text{tr}(\hat{C}_{\mathbf{n}} \hat{\rho}_{\text{exp.}}) + \text{tr}(\hat{C}_K \hat{\rho}_{\text{exp.}}). \quad (30)$$

These operators are projectors on the Hilbert spaces associated with the expected correlations between the measurement outcomes. For the  $\mathbf{n}$ -correlation operator, this projector can be given by

$$\hat{C}_{\mathbf{n}} = \sum_{\mathbf{n}_m \leq 1} |\mathbf{n} \bar{\mathbf{n}}\rangle \langle \mathbf{n} \bar{\mathbf{n}}|, \quad (31)$$

where each local state is associated with a specific pattern class. It is therefore possible to re-organize the sum into pattern classes, so that the correlations between pattern classes  $\mathbf{p}$  and complementary pattern classes  $\bar{\mathbf{p}}$  are separated from the correlations between pattern shifts  $m$ ,

$$\hat{C}_{\mathbf{n}} = \sum_{\mathbf{p}} \sum_{m=0}^{d_{\mathbf{p}}-1} (\hat{S} \otimes \hat{S})^m |\mathbf{p} \bar{\mathbf{p}}\rangle \langle \mathbf{p} \bar{\mathbf{p}}| (\hat{S}^\dagger \otimes \hat{S}^\dagger)^m. \quad (32)$$

Importantly, the correlation is always zero if the photon number distributions observed in the output belong to different pattern classes. Oppositely, the fidelity of the  $K$ -correlation is completely independent of the pattern class combination. If the sum over pattern classes is separated from the sum over the possible combinations of  $K$  and  $-K$ , the  $K$ -correlation operator reads

$$\hat{C}_K = \sum_{\mathbf{p}_A, \mathbf{p}_B} \sum_K |\mathcal{E}_{\mathbf{p}_A}, K; \mathcal{E}_{\mathbf{p}_B}, -K\rangle \langle \mathcal{E}_{\mathbf{p}_A}, K; \mathcal{E}_{\mathbf{p}_B}, -K|. \quad (33)$$

While this operator also commutes with projections on specific pattern class subspaces, it does have non-zero eigenvalues for non-complementary pattern classes. Experimentally, this reflects the fact that the actual measurement of  $K$  does not distinguish the pattern classes, so that it is impossible to tell which part of the observed  $K$ -correlation originates from which pattern class.

Note that the relations given above are based on the mode shift rule of DFTs, which shows that the eigenspaces of  $K$ -values can be expressed in terms of the eigenstates of the mode shift operation within each pattern class. It is therefore possible to evaluate the correlations between  $K$  within each pattern class, so that the entanglement criterion does not depend on quantum coherences between different pattern classes. To find an experimental criterion for the detection of entanglement, we now consider the maximal fidelity sum that can be obtained with separable inputs,

$$\max_{\text{sep.}}(F_{\mathbf{n}} + F_K) = \max_{\rho_{\text{sep.}}}(\text{tr}((\hat{C}_{\mathbf{n}} + \hat{C}_K)\hat{\rho}_{\text{sep.}})) = B_{\text{sep.}}. \quad (34)$$

If the sum of the correlation fidelities exceeds this boundary, the state  $\hat{\rho}_{\text{exp.}}$  generated in the experiment is definitely entangled.

Since the operators representing the  $\mathbf{n}$ - and  $K$ -correlations both commute with projectors onto the pattern class subspaces, we can express the fidelities as a product of pattern class probability  $P(\mathbf{p}_A, \mathbf{p}_B)$  and the fidelity for the projection of the state into that pattern class combination. Here, the pattern class probability is given by

$$P(\mathbf{p}_A, \mathbf{p}_B) = \text{tr}(\hat{\Pi}_{\mathbf{p}_A, \mathbf{p}_B} \hat{\rho}_{\text{exp.}}) \quad (35)$$

and the conditional pattern class states are given by

$$\hat{R}_{\mathbf{p}_A, \mathbf{p}_B} = \frac{\hat{\Pi}_{\mathbf{p}_A, \mathbf{p}_B} \hat{\rho}_{\text{exp.}} \hat{\Pi}_{\mathbf{p}_A, \mathbf{p}_B}}{P(\mathbf{p}_A, \mathbf{p}_B)}, \quad (36)$$

where  $\hat{\Pi}_{\mathbf{p}_A, \mathbf{p}_B}$  is the projection operator on the  $(\mathbf{p}_A, \mathbf{p}_B)$ -pattern subspace  $\mathbb{H}_{\mathbf{p}_A} \otimes \mathbb{H}_{\mathbf{p}_B}$ . We can then express the Fidelities  $F_{\mathbf{n}}$  and  $F_K$  as an average over the fidelities in the different pattern classes, as given by

$$F_{\mathbf{n}} + F_K = \sum_{\mathbf{p}_A, \mathbf{p}_B} P(\mathbf{p}_A, \mathbf{p}_B) \text{tr}((\hat{C}_{\mathbf{n}} + \hat{C}_K) \hat{R}_{\mathbf{p}_A, \mathbf{p}_B}). \quad (37)$$

Since the maximum of a statistical average cannot be larger than the maximal individual contribution, we can identify all relevant bounds on  $F_{\mathbf{n}} + F_K$  by selecting the pattern class subspace within which the maximal fidelity sum is achieved.

For a separable state  $\hat{R}_{\mathbf{p}_A, \mathbf{p}_B}(\text{sep.})$  in the pattern subspace  $(\mathbf{p}_A, \mathbf{p}_B)$ , the maximal fidelities can be determined using the well established criteria for mutually unbiased bases (MUBs) [48, 49]. A particularly simple case is obtained for  $\mathbf{p}_A \neq \bar{\mathbf{p}}_B$ , where the pattern classes in system  $A$  and system  $B$  are not complementary. In this case,  $F_{\mathbf{n}} = 0$  and  $F_K \leq 1$ , so the sum of the fidelities cannot exceed one for any state, entangled or separable. The maximal value of  $F_{\mathbf{n}} + F_K = 2$  associated with the ideal entangled state can only be achieved in complementary pattern classes. For separable states  $\hat{R}_{\mathbf{p}, \bar{\mathbf{p}}}(\text{sep.})$  in complementary pattern subspaces, the photon number basis and the  $K$ -basis are mutually unbiased and the upper bound of the fidelity sum is given by

$$\text{tr}((\hat{C}_{\mathbf{n}} + \hat{C}_K) \hat{R}_{\mathbf{p}, \bar{\mathbf{p}}}(\text{sep.})) \leq 1 + \frac{1}{d_{\mathbf{p}}}, \quad (38)$$

where  $d_{\mathbf{p}}$  is the cardinality of the  $\mathbf{p}$ -pattern class.

According to Eq. (37), the fidelities for arbitrary states are obtained by averaging over the fidelities of the contributions from different pattern spaces. Thus the highest possible value of  $F_{\mathbf{n}} + F_K$  is achieved by a separable state from the subspace of complementary pattern classes  $(\mathbf{p}, \bar{\mathbf{p}})$  with the lowest possible cardinality  $d_{\mathbf{p}}$ . As a result, the upper bound of the fidelity sum for all separable states is given by

$$\max_{\text{sep.}}(F_{\mathbf{n}} + F_K) = 1 + \frac{1}{\min_{\mathbf{p}} d_{\mathbf{p}}}. \quad (39)$$

As mentioned above, any state that exceeds this bound is necessarily entangled. We can therefore verify the bipartite entanglement between the two multi-mode systems at  $A$  and at  $B$  by evaluating the correlations between photon distributions detected in the input modes and the correlations between the  $K$ -values of the photon distributions detected in the output modes of a DFT. If the experimentally determined values exceed the bound given by Eq.(39) the generation of entanglement between the two multi-mode systems has been verified.

The upper bound derived above makes no use of any information about the actual pattern class distribution of the generated state. This may be a significant disadvantage when most pattern classes of the state have a much higher cardinality than the minimal cardinality used for the bound. It may therefore be useful to consider the actual distribution of cardinalities of pattern classes for a specific number of modes  $M$ . Specifically, a cardinality of  $d_{\mathbf{p}} = M$  means that the photon number distribution  $\mathbf{p}$  is different for each mode shift, while a cardinality of  $d_{\mathbf{p}} = M/\nu$  means that the photon number distribution  $\mathbf{p}$  returns to the original distribution after only  $M/\nu$  mode shifts because the same pattern is repeated  $\nu$  times along the  $M$  modes. Existence of pattern classes with lower cardinalities thus requires that  $M$  can be factorized into  $\nu$  and  $M/\nu$ . If the total photon number  $M$  is a prime number, then every local pattern class has the cardinality  $M$  and the upper bound in Eq. (39) is optimal for every local pattern classes  $(\mathbf{p}_A, \mathbf{p}_B)$ . However, prime numbers are less and less common as the number of modes increases, so that a limitation to prime numbers may be inconvenient. In addition, an even number of modes (or even a power of two for the number of modes) may be convenient for the design of the experimental setup. We should therefore also consider the worst case scenario, which occurs when an even total photon number  $M$  is split into equal photon numbers of  $(M/2, M/2)$ . The lowest cardinality of a pattern class of  $M/2$  photons in  $M$  modes is the cardinality of 2 of the pattern class  $\mathcal{E}_{1010\dots10}$  which is complementary to itself. In this case, the bound derived above is definitely far from optimal, resulting in a maximal value of  $3/2$  that is only achieved by separable states from the two dimensional subspaces of a single pattern class. It is easy to see from the correlation measurements of the input photon number distributions that only a very small fraction of the photons is found in this very small pattern class. We should therefore consider an improvement of the bound that includes the actual pattern class statistics observed in the experiment.



## 7. Tighter bounds based on pattern class statistics

As mentioned above, we actually obtain detailed information about the pattern class distribution in the photon detection measurement of the input modes. As a consequence, we can determine the probability distribution  $P(\mathbf{p}_A, \mathbf{p}_B)$  from the experimental data. Based on this probability distribution, the worst case scenario is a mixture of separable states from each pattern class combination that achieves the bound for that pattern class. By including this experimental evidence, we find the tighter bound

$$\max_{\text{sep.}}(F_n + F_K) = 1 + \sum_{\mathbf{p}} \frac{1}{d_{\mathbf{p}}} P(\mathbf{p}, \bar{\mathbf{p}}). \quad (40)$$

Note that the bound is one if the pattern classes are not complementary, so it is sufficient to sum over the increases of the bound for the different complementary pattern classes. The bound above can be achieved by a mixture of correlated product states  $|\mathbf{n}, \bar{\mathbf{n}}\rangle$  which achieve  $F_n = 1$  and  $F_K = 1/d_{\mathbf{p}}$  in their respective pattern class  $(\mathbf{p}, \bar{\mathbf{p}})$ . Interestingly, this bound is also achieved by product states of photon number distributions in the output modes of the DFT, where  $F_K = 1$  and the pattern classes are randomly distributed and uncorrelated. However, the probability of accidentally finding the complementary pattern in  $(\mathbf{p}, \bar{\mathbf{p}})$  is exactly  $1/d_{\mathbf{p}}$ , satisfying the bound of Eq.(40).

Since the pattern class statistics is part of the experimental result, it is not actually part of the bound itself and should be moved to the left side of the relation, along with the two fidelities. For this purpose we define the statistical pattern class defect  $D_{\mathbf{p}}$  as the average value of  $1/d_{\mathbf{p}}$  obtained from the experimentally observed distribution of pattern classes,

$$D_{\mathbf{p}} = \sum_{\mathbf{p}} \frac{1}{d_{\mathbf{p}}} P(\mathbf{p}, \bar{\mathbf{p}}). \quad (41)$$

By including the pattern class defect in the experimental evaluation of the quantum state, we can formulate a new bound on separable states that reads

$$\max_{\text{sep.}}(F_n - D_{\mathbf{p}} + F_K) = 1. \quad (42)$$

It is also possible to express the pattern class defect  $D_{\mathbf{p}}$  as the expectation value of an operator,

$$D_{\mathbf{p}} = \text{tr}(\hat{C}_{\mathbf{p}} \rho_{\text{exp.}}) = \text{tr} \left( \rho_{\text{exp.}} \sum_{\mathbf{p}: n_m \leq 1} \frac{1}{d_{\mathbf{p}}} \hat{\Pi}_{\mathbf{p}, \bar{\mathbf{p}}} \right), \quad (43)$$

where the sum runs over all the local pattern classes  $\mathbf{p}$  that have corresponding complementary pattern class, i.e. the photon number in each mode does not exceeds 1,  $n_m \leq 1$ . For completeness, we can also express the entanglement criterion by a witness operator  $\hat{W}$ , defined so that any positive expectation value of  $\hat{W}$  indicates entanglement. In terms of the operators defined previously, this entanglement witness is given by

$$\hat{W} = \hat{C}_n - \hat{C}_{\mathbf{p}} + \hat{C}_K - \mathbb{1}. \quad (44)$$

The maximal eigenvalues of this entanglement witness are associated with the pattern classes of maximal cardinality,  $d_{\mathbf{p}} = M$ . Within each pattern class of maximal cardinality  $M$ , there exists a maximally entangled eigenstate of  $\hat{W}$  with the maximal eigenvalue of  $1 - 1/M$ .

For the intended entangled state  $|\phi_{N,M-N}\rangle$ , the expectation value of the witness operator  $\hat{W}$  is actually lower than the maximal eigenvalue, since the state is not limited to specific pattern classes. Since the state includes pattern classes with lower cardinality, it is not an eigenstate of  $\hat{W}$  and has an expectation value that is somewhat lower than the maximal eigenvalue of  $1 - 1/M$ . Specifically, the expectation value is given by

$$\langle \phi_{N,M-N} | \hat{W} | \phi_{N,M-N} \rangle = 1 - \sum_{\mathbf{p}: n_m \leq 1} \frac{1}{d_{\mathbf{p}}} \langle \phi_{N,M-N} | \hat{\Pi}_{\mathbf{p},\bar{\mathbf{p}}} | \phi_{N,M-N} \rangle, \quad (45)$$

where the probability of each pattern class with  $n_m \leq 1$  is proportional to its cardinality  $d_{\mathbf{p}}$ , so that each pattern class reduces the expectation value of the witness by the same amount,

$$\frac{1}{d_{\mathbf{p}}} \langle \phi_{N,M-N} | \hat{\Pi}_{\mathbf{p},\bar{\mathbf{p}}} | \phi_{N,M-N} \rangle = \frac{1}{\binom{M}{N}}. \quad (46)$$

Effectively, the average value of  $1/d_{\mathbf{p}}$  is given by the ratio of the number of local pattern classes with  $n_m \leq 1$  and the total number of local photon distributions with  $n_m \leq 1$ . As photon number increases, this average  $D_{\mathbf{p}}$  is expected to converge on  $1/M$ , since the vast majority of pattern classes has a cardinality of  $M$ .

## 8. Entanglement between two systems with two photons in four modes

In this section, we will illustrate the principles explained above using the most simple non-trivial case of  $M = 4$  single photon inputs, where two photons are distributed to  $A$  and two photons are distributed to  $B$ . Before the post-selection of  $N = 2$ , the state is given by a superposition of the different photon number partitions,

$$|\psi_{M=4}\rangle = \frac{1}{4} \left( |\phi_{0A,4B}\rangle + |\phi_{4A,0B}\rangle + 2|\phi_{1A,3B}\rangle + \sqrt{6}|\phi_{2A,2B}\rangle + 2|\phi_{3A,1B}\rangle \right). \quad (47)$$

Since we are using linear optics and photon detection, we will always distinguish the different photon number partitions from each other. The probability of obtaining a completely useless output with zero photons in either  $A$  or  $B$  is  $1/8$ . The probability of getting a  $4 \times 4$  entangled state of one photon entangled with three photons is  $1/2$ . In this case, there is a single pattern class in the system with one photon, and the information contributed by the multi-photon patterns in the other system is generally redundant. Thus the most interesting output is the distribution of two photons to each system, which occurs with a probability of  $3/8$ . However, it might be worth noting that the probability of generating usable entanglement from four single photon inputs is  $7/8$ , which means that single photon sources can be used to generate entanglement on demand with a success rate that is almost as high as the success rate of the initial

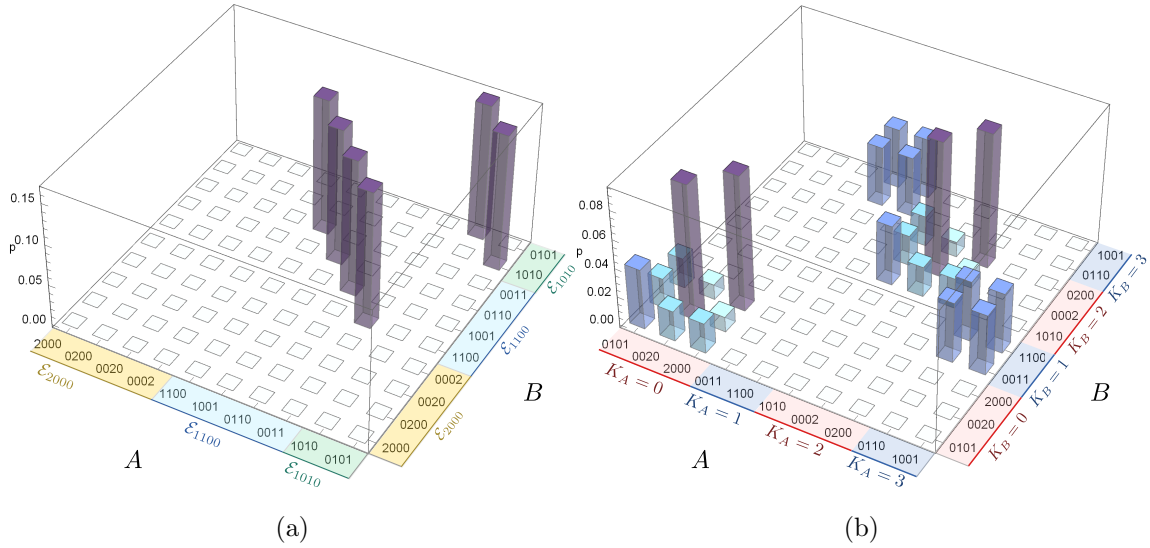


**Figure 3.** The probability distribution of photon number detection events for the state  $|\phi_{2A,2B}\rangle$  (a) in the original input modes and (b) in the output modes of local DFTs. The axes labeled  $A$  and  $B$  show the photon distributions detected in each local system. In (a), the photon distributions have been arranged according to the maximal number of photons in one mode (Eq. (49)). In (b), the distributions have been organized according to the  $K$ -value (Eq. (50)). The first three outcomes correspond to  $K = 0$ , the next two outcomes have  $K = 1$ , followed by another block of three outcomes with  $K = 2$  and finally two outcomes with  $K = 3$ . The outcomes are clearly grouped in correlated blocks corresponding to the expected correlations in  $K$ .

single photon generation. In the light of the rather low success rates associated with most post-selected linear optics quantum circuits, this seems to be a noteworthy result.

We now focus on the output state  $|\phi_{2A,2B}\rangle$ , which is an entangled state with a Schmidt rank of 6, as seen in the superposition of local input mode states,

$$\begin{aligned}
 |\phi_{2A,2B}\rangle = \frac{1}{\sqrt{6}} (&|1100\rangle|0011\rangle + |0110\rangle|1001\rangle + |0011\rangle|1100\rangle + |1001\rangle|0110\rangle \\
 &+ |1010\rangle|0101\rangle + |0101\rangle|1010\rangle).
 \end{aligned}
 \tag{48}$$

The photon number distribution of this state in the input modes is shown in Fig. 3(a). In total, there are ten possible output distributions, corresponding to the possible distributions of two photons in four modes. In Fig. 3(a) these are arranged according to the three cyclic pattern classes  $\mathbf{p} = 2000, 1100, 1010$ , which have the following elements

$$\begin{aligned}
 \mathcal{E}_{2000} &= \{|2000\rangle, |0200\rangle, |0020\rangle, |0002\rangle\}, \\
 \mathcal{E}_{1100} &= \{|1100\rangle, |0110\rangle, |0011\rangle, |1001\rangle\}, \\
 \mathcal{E}_{1010} &= \{|1010\rangle, |0101\rangle\}.
 \end{aligned}
 \tag{49}$$

The photon number outputs in  $A$  and  $B$  are perfectly correlated in the six

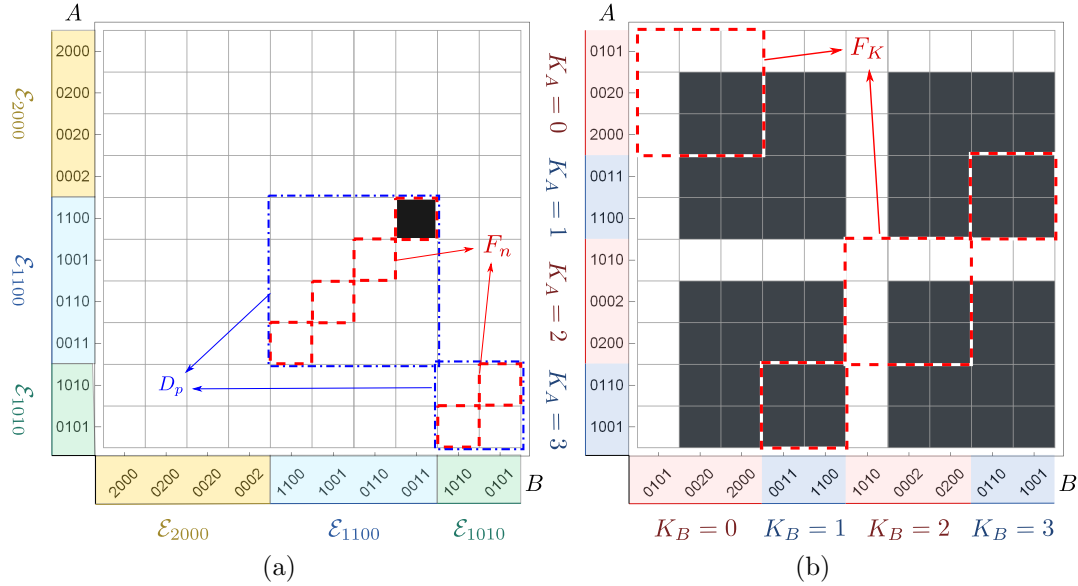


**Figure 4.** The statistics of photon number detection of the separable state  $|1100_A, 0011_B\rangle$  (a) in the input modes and (b) in the output modes of two local DFTs. Photon distributions are arranged in the same way as in Fig. 3. The red dashed squares show outputs that have the correct correlation expected from the entangled state input  $|\phi_{2A,2B}\rangle$  and therefore contribute to the fidelities  $F_n$  or  $F_K$ , respectively. The blue dot-dashed squares indicate the complementary pattern classes  $(\mathbf{p}, \bar{\mathbf{p}})$  which are used to determine the tighter bounds for separable states. In (a), the separable input state corresponds to a well-defined measurement outcome with  $F_n = 1$  and  $P(\mathcal{E}_{1100}, \mathcal{E}_{0011}) = 1$ . In the output modes of the DFT, the photon number distributions shown by the black squares in (b) each have a probability of 1/64. As a result, the  $K$ -correlation fidelity, i.e. the probability for the  $(K, -K)$ -correlations (red dashed squares) is  $F_K = 1/4$ .

complementary pattern pairs  $(\mathbf{n}, \bar{\mathbf{n}})$  with maximally one photon in each mode. The four patterns with two photons in the same mode have a detection probability of zero.

If the photons are detected in the output modes of two local DFTs, all possible output patterns will be observed. The probabilities of the different output distributions are shown in Fig. 3(b). Here, the correlation is between  $K$ -values, so it is convenient to arrange the output distributions accordingly. The photon distributions with the same  $K$ -value are

$$\begin{aligned} \mathcal{E}_{K=0} &= \{|0101\rangle, |2000\rangle, |0020\rangle\}, & \mathcal{E}_{K=1} &= \{|0011\rangle, |1100\rangle\}, \\ \mathcal{E}_{K=2} &= \{|1010\rangle, |0200\rangle, |0002\rangle\}, & \mathcal{E}_{K=3} &= \{|0110\rangle, |1001\rangle\}. \end{aligned} \quad (50)$$

As can be seen in Fig. 3(b), the  $K$ -values are correlated to that the sum of the  $K$ -values is zero or four. Specifically, there are four blocks corresponding to  $K$ -values of  $(0, 0)$ ,  $(1, 3)$ ,  $(2, 2)$  and  $(3, 1)$ . The remaining 12 combinations all have a probability of zero.

We can now compare the statistics of the entangled state with the statistics obtained from a separable state with  $F_n = 1$ . Fig. 4 illustrates the statistics obtained with the product state  $|1100_A, 0011_B\rangle$  from the pattern class  $\mathcal{E}_{1100}$ , which is complementary to

itself. Fig. 4 (a) shows the photon number distribution associated with this state as a black square. The red dashed lines indicate the results obtained from the ideal entangled state  $|\phi_{2_A,2_B}\rangle$  and the blue dot-dashed squares identify the combinations of complementary pattern classes associated with the entangled state  $|\phi_{2_A,2_B}\rangle$ . There are two pattern classes, both of which are complementary to themselves. The separable state is located in the larger pattern class, so that its value of  $D_{\mathbf{p}}$  is  $1/4$ . For the entangled state  $|\phi_{2_A,2_B}\rangle$ , the value is actually higher, since there are two pattern classes and six photon number combinations, resulting in a  $D_{\mathbf{p}}$  value of  $1/3$ . Fig. 4 (b) shows the photon distribution of the separable state in the output modes of the DFT. In general, photon number states in the input modes have a completely random distribution of  $K$ -values. In the specific case of the  $|1100_A, 0011_B\rangle$  state we find 64 outcomes with equal probabilities of  $1/64$  each, as indicated by the black squares in Fig. 4 (b). The red dashed squares indicate the results with  $K_A + K_B = 0$ . Since the  $K$ -values of the local state are completely uncorrelated and equally distributed over  $K = 0, 1, 2, 3$ , the probability of finding the correct correlation is  $F_K = 1/4$ . As expected, this is exactly equal to the tighter bound for separable states,  $F_{\mathbf{n}} - D_{\mathbf{p}} + F_K = 1$ . Fig. 4 thus illustrates how a separable state achieves the bound given by Eq. (42).

The entanglement criterion applies to experimental data obtained under non-ideal circumstances. It is therefore interesting to evaluate the robustness of the state  $|\phi_{2_A,2_B}\rangle$  to potential error sources. In the absence of a specific error model, it is possible to evaluate the robustness in terms of the quantum state fidelity  $F_{\text{state}}$ . Since the correlation fidelities  $F_{\mathbf{n}}$  and  $F_K$  for the target state are both 1, which contributes a fraction of  $F_{\text{state}}$  to the statistics, while the correlation fidelities for the errors have the minimum value of 0, the quantum state fidelity provides a lower bound for both fidelities. Therefore we find that

$$\min(F_{\mathbf{n}} + F_K) = 2F_{\text{state}} \quad (51)$$

If we apply the entanglement criterion of Eq.(39) to the present case, the limit for separable states is

$$\min(F_{\mathbf{n}} + F_K) = 3/2. \quad (52)$$

We find that this limit is always exceeded when  $F_{\text{state}} > 3/4$ . Thus a quantum state fidelity of more than 75 percent guarantees entanglement verification using the basic entanglement criterion of Eq.(39). Note that the sufficiency of 75 percent fidelity for entanglement is derived from the worst case scenario that the total mode number  $M = 4$  is an even number. A quantum state fidelity of 75 percent therefore guarantees the entanglement between  $A$  and  $B$  for arbitrary post-selected bipartite systems with  $N$  photons at local system  $A$  and  $M - N$  photons at local system  $B$ .

A more specific analysis is necessary to determine the quantum state fidelity at which the tighter bound of Eq.(42) will be exceeded. Here, we have to take into account the pattern class distribution and the associated values of  $D_{\mathbf{p}}$ . As shown above, the ideal state has  $D_{\mathbf{p}} = 1/3$  and hence the quantity  $F_{\mathbf{n}} - D_{\mathbf{p}} + F_K$  has the value  $5/3$  for the ideal component  $|\phi_{2_A,2_B}\rangle$ , which contributes a fraction of  $F_{\text{state}}$  to the

statistics. Here, we also need to consider the possible contributions to  $D_{\mathbf{p}}$  by the error statistics. However, the error statistics may contribute a different value of  $D_{\mathbf{p}}$ . The most conservative assumption that the errors originates from the smallest complementary pattern class ( $\mathcal{E}_{1010}, \mathcal{E}_{0101}$ ) would assign the maximal value  $D_{\mathbf{p}} = 1/2$  to all of the errors, and the quantity  $F_{\mathbf{n}} - D_{\mathbf{p}} + F_K$  has the lower bound  $-1/2$ , which contributes a fraction of  $1 - F_{\text{state}}$  to the statistics. This resulting in a bound of

$$\min(F_{\mathbf{n}} - D_{\mathbf{p}} + F_K) = \frac{13}{6}F_{\text{state}} - \frac{1}{2}. \quad (53)$$

From this bound, we find that a quantum state fidelity of  $F_{\text{state}} > 9/13$  is sufficient for an experimental verification of entanglement using the criterion of Eq. (39). In terms of the numerical value, this is a quantum state fidelity of about 69.23 percent.

Finally, it may also be worth noting that the expectation value of the witness operator  $\hat{W}$  for a completely random state  $\hat{\rho} = \hat{1}/100$  can be obtained from Fig. 4 by counting the number of outcomes in the red dashed squares. The results are 0.06 for the fidelity  $F_{\mathbf{n}}$ , 0.26 for the fidelity  $F_K$ , and 0.06 for the pattern class defect  $D_{\mathbf{p}}$ . Therefore, the expectation value of  $\hat{W}$  for a completely random state is  $-0.74$ . For the ideal state, the expectation value of the witness is  $2/3 \approx 0.67$ . For a statistical mixture of the random state and the ideal state given by

$$\hat{\rho} = p |\phi_{2_A, 2_B}\rangle \langle \phi_{2_A, 2_B}| + (1 - p) \frac{1}{100} \mathbb{1}, \quad (54)$$

the expectation value of the entanglement witness  $\hat{W}$  is therefore given by  $1.41p - 0.74$ , which exceeds zero for  $p > 0.525$ . We can therefore conclude that the experimental entanglement criterion given by Eq. ((42)) and the corresponding entanglement witness  $\hat{W}$  can detect entanglement even when about 45 percent of the state are completely randomized.

## 9. Conclusion

In conclusion, we have presented a practical method of evaluating the entanglement between two local multi-mode systems that can be generated and scaled up easily if sufficiently reliable single photon sources and linear optics circuits are available. The mode shift rule of the discrete Fourier transform (DFT) allows us to keep track of the quantum mechanical complementarity between multi-photon distributions observed in the input modes and in the output modes of a DFT. This means that we can simplify the analysis of the large and increasingly complex Hilbert spaces of large photon numbers distributed over an equally large number of modes. We have shown that the entanglement criteria based on the evaluation of the two complementary photon detection statistics obtained from the original input modes and from the output modes of the DFT is sufficiently tight and robust to permit the experimental verification of the entanglement in the presence of imperfections. Specifically, we find that a quantum state

fidelity above 75 percent is sufficient for a straightforward verification of entanglement based on the sum of the correlation fidelities obtained from the two measurements.

The present work provides the necessary tools for the characterization and control of entanglement between multi-mode systems with high photon numbers. It thus opens up new possibilities for the generation and application of quantum states in large scale systems. Since much effort is currently made to increase the size of optical quantum circuits, both in terms of the number of modes and in the number of photons, the present work may serve as a guide to the new territory pioneered by these technological advances. The concepts developed should provide helpful examples of how to address the increasing complexity of large scale quantum systems. In particular, the DFT and its mode shift rule appear to be an important and highly versatile element in the quantum optical toolbox for the development of future quantum technologies. We therefore hope that the present work provides a useful starting point for a more detailed exploration of the wide variety of new experimental possibilities that are beginning to emerge as a result of ongoing research in the field.

## Acknowledgments

This work was supported by JSPS KAKENHI Grant Number 26220712.

- [1] Eisenberg H S, Khoury G, Durkin G A, Simon C and Bouwmeester D 2004 *Phys. Rev. Lett.* **93**(19) 193901 URL <http://link.aps.org/doi/10.1103/PhysRevLett.93.193901>
- [2] Nagata T, Okamoto R, O'Brien J L, Sasaki K and Takeuchi S 2007 *Science* **316** 726–729
- [3] Matthews J C F, Politi A, Stefanov Andre and O'Brien J L 2009 *Nat Photon* **3** 346–350 ISSN 1749-4885 URL <http://dx.doi.org/10.1038/nphoton.2009.93>
- [4] Bogdanov Y I, Chekhova M V, Kulik S P, Maslennikov G A, Zhukov A A, Oh C H and Tey M K 2004 *Phys. Rev. Lett.* **93**(23) 230503 URL <http://link.aps.org/doi/10.1103/PhysRevLett.93.230503>
- [5] Wiecek W, Krischek R, Kiesel N, Michelberger P, Tóth G and Weinfurter H 2009 *Phys. Rev. Lett.* **103**(2) 020504 URL <http://link.aps.org/doi/10.1103/PhysRevLett.103.020504>
- [6] Afek I, Ambar O and Silberberg Y 2010 *Science* **328** 879–881 ISSN 0036-8075 (*Preprint* <http://science.sciencemag.org/content/328/5980/879.full.pdf>) URL <http://science.sciencemag.org/content/328/5980/879>
- [7] Wang H, Marantoni M, Bialczak R C, Lenander M, Lucero E, Neeley M, O'Connell A D, Sank D, Weides M, Wenner J, Yamamoto T, Yin Y, Zhao J, Martinis J M and Cleland A N 2011 *Phys. Rev. Lett.* **106**(6) 060401 URL <http://link.aps.org/doi/10.1103/PhysRevLett.106.060401>
- [8] Xiang G Y, Hofmann H F and Pryde G J 2013 *Scientific Reports* **3** 2684– URL <http://dx.doi.org/10.1038/srep02684>
- [9] Israel Y, Afek I, Rosen S, Ambar O and Silberberg Y 2012 *Phys. Rev. A* **85**(2) 022115 URL <http://link.aps.org/doi/10.1103/PhysRevA.85.022115>
- [10] Takeuchi S, Okamoto R and Sasaki K 2004 *Appl. Opt.* **43** 5708–5711 URL <http://ao.osa.org/abstract.cfm?URI=ao-43-30-5708>
- [11] U'Ren A B, Silberhorn C, Banaszek K and Walmsley I A 2004 *Phys. Rev. Lett.* **93**(9) 093601 URL <http://link.aps.org/doi/10.1103/PhysRevLett.93.093601>
- [12] Ates S, Agha I, Gulinatti A, Rech I, Rakher M T, Badolato A and Srinivasan K 2012 *Phys. Rev. Lett.* **109**(14) 147405 URL <http://link.aps.org/doi/10.1103/PhysRevLett.109.147405>
- [13] Bernien H, Childress L, Robledo L, Markham M, Twitchen D and Hanson R 2012 *Phys. Rev. Lett.* **108**(4) 043604 URL <http://link.aps.org/doi/10.1103/PhysRevLett.108.043604>

- [14] Sanaka K, Pawlis A, Ladd T D, Lischka K and Yamamoto Y 2009 *Phys. Rev. Lett.* **103**(5) 053601  
URL <http://link.aps.org/doi/10.1103/PhysRevLett.103.053601>
- [15] Santori C, Fattal D, Vučković J, Solomon G S and Yamamoto Y 2002 *Nature* **419** 594–597
- [16] Kuhn A, Hennrich M and Rempe G 2002 *Phys. Rev. Lett.* **89**(6) 067901 URL <http://link.aps.org/doi/10.1103/PhysRevLett.89.067901>
- [17] Keller M, Lange B, Hayasaka K, Lange W and Walther H 2004 *Nature* **431** 1075–1078
- [18] Mücke M, Bochmann J, Hahn C, Neuzner A, Nölleke C, Reiserer A, Rempe G and Ritter S 2013 *Phys. Rev. A* **87**(6) 063805 URL <http://link.aps.org/doi/10.1103/PhysRevA.87.063805>
- [19] Eisaman M D, Fan J, Migdall A and Polyakov S V 2011 *Review of Scientific Instruments* **82** 071101  
URL <http://scitation.aip.org/content/aip/journal/rsi/82/7/10.1063/1.3610677>
- [20] Takeuchi S 2014 *Japanese Journal of Applied Physics* **53** 030101 URL <http://stacks.iop.org/1347-4065/53/i=3/a=030101>
- [21] Reck M, Zeilinger A, Bernstein H J and Bertani P 1994 *Phys. Rev. Lett.* **73**(1) 58–61 URL <https://link.aps.org/doi/10.1103/PhysRevLett.73.58>
- [22] Weihs G, Reck M, Weinfurter H and Zeilinger A 1996 *Opt. Lett.* **21** 302–304 URL <http://ol.osa.org/abstract.cfm?URI=ol-21-4-302>
- [23] Walborn S P, de Oliveira A N, Pádua S and Monken C H 2003 *Phys. Rev. Lett.* **90**(14) 143601  
URL <https://link.aps.org/doi/10.1103/PhysRevLett.90.143601>
- [24] Barak R and Ben-Aryeh Y 2007 *J. Opt. Soc. Am. B* **24** 231–240 URL <http://josab.osa.org/abstract.cfm?URI=josab-24-2-231>
- [25] Peruzzo A, Laing A, Politi A, Rudolph T and O'Brien J L 2011 *Nature Communications* **2** 224–  
URL <http://dx.doi.org/10.1038/ncomms1228>
- [26] Spagnolo N, Aparo L, Vitelli C, Crespi A, Ramponi R, Osellame R, Mataloni P and Sciarrino F 2012 *Scientific Reports* **2** 862– URL <http://dx.doi.org/10.1038/srep00862>
- [27] Metcalf B J, Thomas-Peter N, Spring J B, Kundys D, Broome M A, Humphreys P C, Jin X M, Barbieri M, Steven Kolthammer W, Gates J C, Smith B J, Langford N K, Smith P G and Walmsley I A 2013 *Nature Communications* **4** 1356– URL <http://dx.doi.org/10.1038/ncomms2349>
- [28] Chaboyer Z, Meany T, Helt L G, Withford M J and Steel M J 2015 *Scientific Reports* **5** 9601–  
URL <http://dx.doi.org/10.1038/srep09601>
- [29] Aaronson S and Arkhipov A 2011 The computational complexity of linear optics *Proceedings of the Forty-third Annual ACM Symposium on Theory of Computing STOC '11* (New York, NY, USA: ACM) pp 333–342 ISBN 978-1-4503-0691-1 URL <http://doi.acm.org/10.1145/1993636.1993682>
- [30] Crespi A, Osellame R, Ramponi R, Brod D J, Galvao E F, Spagnolo N, Vitelli C, Maiorino E, Mataloni P and Sciarrino F 2013 *Nat Photon* **7** 545–549 ISSN 1749-4885 URL <http://dx.doi.org/10.1038/nphoton.2013.112>
- [31] Spring J B, Metcalf B J, Humphreys P C, Kolthammer W S, Jin X M, Barbieri M, Datta A, Thomas-Peter N, Langford N K, Kundys D, Gates J C, Smith B J, Smith P G R and Walmsley I A 2013 *Science* **339** 798–801 ISSN 0036-8075 (*Preprint* <http://science.sciencemag.org/content/339/6121/798.full.pdf>) URL <http://science.sciencemag.org/content/339/6121/798>
- [32] Ralph T C 2013 *Nat Photon* **7** 514–515 ISSN 1749-4885 URL <http://dx.doi.org/10.1038/nphoton.2013.175>
- [33] Humphreys P C, Barbieri M, Datta A and Walmsley I A 2013 *Phys. Rev. Lett.* **111**(7) 070403  
URL <https://link.aps.org/doi/10.1103/PhysRevLett.111.070403>
- [34] Wiseman H M and Vaccaro J A 2003 *Phys. Rev. Lett.* **91**(9) 097902 URL <http://link.aps.org/doi/10.1103/PhysRevLett.91.097902>
- [35] Scheel S 2004 (*Preprint* [quant-ph/0406127](https://arxiv.org/abs/quant-ph/0406127)) URL <https://arxiv.org/abs/quant-ph/0406127>
- [36] Tichy M C, Tiersch M, de Melo F, Mintert F and Buchleitner A 2010 *Phys. Rev. Lett.* **104**(22) 220405  
URL <http://link.aps.org/doi/10.1103/PhysRevLett.104.220405>



- [37] Spagnolo N, Vitelli C, Sansoni L, Maiorino E, Mataloni P, Sciarrino F, Brod D J, Galvão E F, Crespi A, Ramponi R and Osellame R 2013 *Phys. Rev. Lett.* **111**(13) 130503 URL <https://link.aps.org/doi/10.1103/PhysRevLett.111.130503>
- [38] Crespi A, Osellame R, Ramponi R, Bentivegna M, Flamini F, Spagnolo N, Viggianiello N, Innocenti L, Mataloni P and Sciarrino F 2016 *Nat Commun* **7** – URL <http://dx.doi.org/10.1038/ncomms10469>
- [39] Valiant L 1979 *Theoretical Computer Science* **8** 189 – 201 ISSN 0304-3975 URL <http://www.sciencedirect.com/science/article/pii/0304397579900446>
- [40] Aaronson S 2011 *Proceedings of the Royal Society of London A: Mathematical, Physical and Engineering Sciences* **467** 3393–3405 ISSN 1364-5021 (*Preprint* <http://rspa.royalsocietypublishing.org/content/467/2136/3393.full.pdf>) URL <http://rspa.royalsocietypublishing.org/content/467/2136/3393>
- [41] Tan S M, Walls D F and Collett M J 1991 *Phys. Rev. Lett.* **66**(3) 252–255 URL <http://link.aps.org/doi/10.1103/PhysRevLett.66.252>
- [42] Hardy L 1994 *Phys. Rev. Lett.* **73**(17) 2279–2283 URL <http://link.aps.org/doi/10.1103/PhysRevLett.73.2279>
- [43] Hessmo B, Usachev P, Heydari H and Björk G 2004 *Phys. Rev. Lett.* **92**(18) 180401 URL <http://link.aps.org/doi/10.1103/PhysRevLett.92.180401>
- [44] van Enk S J 2005 *Phys. Rev. A* **72**(6) 064306 URL <http://link.aps.org/doi/10.1103/PhysRevA.72.064306>
- [45] van Enk S J 2006 *Phys. Rev. A* **74**(2) 026302 URL <http://link.aps.org/doi/10.1103/PhysRevA.74.026302>
- [46] Ou Z Y and Mandel L 1988 *Phys. Rev. Lett.* **61**(1) 50–53 URL <http://link.aps.org/doi/10.1103/PhysRevLett.61.50>
- [47] Tichy M C, Tiersch M, Mintert F and Buchleitner A 2012 *New Journal of Physics* **14** 093015 URL <http://stacks.iop.org/1367-2630/14/i=9/a=093015>
- [48] Wu S, Yu S and Mølmer K 2009 *Phys. Rev. A* **79**(2) 022104 URL <http://link.aps.org/doi/10.1103/PhysRevA.79.022104>
- [49] Spengler C, Huber M, Brierley S, Adaktylos T and Hiesmayr B C 2012 *Phys. Rev. A* **86**(2) 022311 URL <http://link.aps.org/doi/10.1103/PhysRevA.86.022311>